processes

MDPI

Article

Heat Transfer Improvement in MHD Natural Convection Flow of Graphite Oxide/Carbon Nanotubes-Methanol Based Casson Nanofluids Past a Horizontal Circular Cylinder

Abdulkareem Saleh Hamarsheh [1,*], Firas A. Alwawi [1,2], Hamzeh T. Alkasasbeh [3], Ahmed M. Rashad [4] and Ruwaidiah Idris [2]

1 Department of Mathematics, College of Sciences and Humanities in Al-Kharj, Prince Sattam bin Abdulaziz University, Al-Kharj 11942, Saudi Arabia; f.alwawi@psau.edu.sa
2 Faculty of Ocean Engineering Technology and Informatics, Universiti Malaysia Terengganu, Kuala Nerus 21030, Malaysia; ruwaidiah@umt.edu.my
3 Department of Mathematics, Faculty of Science, Ajloun National University, Ajloun 26810, Jordan; alkasasbehh@gmail.com
4 Department of Mathematics, Faculty of Science, Aswan University, Aswan 81528, Egypt; am_rashad@yahoo.com
* Correspondence: a.hamarsheh@psau.edu.sa

Received: 24 October 2020; Accepted: 9 November 2020; Published: 11 November 2020

check for updates

Abstract: This numerical investigation intends to present the impact of nanoparticles volume fraction, Casson, and magnetic force on natural convection in the boundary layer region of a horizontal cylinder in a Casson nanofluid under constant heat flux boundary conditions. Methanol is considered as a host Casson fluid. Graphite oxide (GO), single and multiple walls carbon nanotubes (SWCNTs and MWCNTs) nanoparticles have been incorporated to support the heat transfer performances of the host fluid. The Keller box technique is employed to solve the transformed governing equations. Our numerical findings were in an excellent agreement with the preceding literature. Graphical results of the effect of the relevant parameters on some physical quantities related to examine the behavior of Casson nanofluid flow were obtained, and they confirmed that an augmentation in Casson parameter results in a decline in local skin friction, velocity, or temperature, as well as leading to an increment in local Nusselt number. Furthermore, MWCNTs are the most efficient in improving the rate of heat transfer and velocity, and they possess the lowest temperature.

Keywords: Casson nanofluid; CNTs; constant heat flux; GO; MHD; horizontal circular cylinder; methanol

1. Introduction

The significance of convection from a cylindrical geometry lies in the fact that they are used in numerous physical and engineering applications; these wide usages made researchers direct their great efforts towards this problem. Blasius and Frossling [1,2] solved the momentum and energy equations of combined convection from a horizontal cylinder, respectively. Merkin [3,4] obtained the exact solution for free and combined convection past a horizontal cylinder. Since then, this topic has been extended to include many cases in Newtonian or non-Newtonian fluids, in mixed, forced, or free convection, and many other cases. Merkin and Pop [5] addressed the free convection of viscous fluid about a circular cylinder with prescribed heat flux. Nazar et al. [6] investigated the combined convection flow of micropolar fluid around a circular cylinder. Anwar et al. [7] illustrated the combined convection from a cylinder in a viscoelastic fluid. Mabood et al. [8] analyzed the forced convection flow of nanofluid about a cylinder taken into account convective boundary condition. Roa et al. [9] examined Magnetohydrodynamic (MHD) free convection flow of Williamson non-Newtonian fluid around a circular cylinder considering Newtonian heating. However, it is well known that the rate of heat transfer may be enhanced depending on the geometry and operating conditions. For more reading, see the following references [10–17].

Magnetohydrodynamics (MHD) is a concept that joins three parts: magneto meaning magnetic, hydro that indicates fluid, and dynamic that refers to motion. Accordingly, it can be defined as the study concerned with exploring the effects of crossing a magnetic field within a moving electrically conducting fluid. Magnetic field influences can be observed in many natural phenomena and industrial processes. In the metallurgical industry, the magnetic field is applied to move, pump, and heat molten metals. The Earth's magnetic field that preserves the surface from lethal radiation is produced by the movement of the earth's molten core. Sunspots and solar flares are induced by the solar and galactic magnetic current that affects the composition of stars from interstellar gas clouds, and many others. In the field of heat transfer through convection, many researchers have been interested in studying the effect of the magnetic field on the behavior of electrically conducting fluids. Chamkha and Aly [18] studied the free convection flow of a nanofluid on a permeable vertical plate under the impact of the Lorentz force field, heat generation. or absorption. Hamad et al. [19] examined the natural convection flow of a nanofluid over a vertical semi-infinite flat plate with MHD effect. Rana et al. [20] employed Buongiorno's model for studying the behavior of water nanofluid flowing over a horizontal shrinking cylinder in the presence of the magnetic field and thermal slip. Alwawi et al. [21] addressed the aspects of heat transfer improvement of carboxymethyl cellulose-water nanofluid over a solid sphere under the impact of Lorentz force.

Nanoparticles are used to improve the thermal conductivity and heat transfer coefficient of conventional fluids. The idea of nanoparticles was first introduced by Choi and Eastman [22]. Akbar et al. [23] numerically investigated the flow of nanofluid past a stretching cylinder under Radiation and magnetic field effects. Dhanai et al. [24] employed Buongiorno's model to investigate MHD combined convection flow of nanofluid about an inclined cylinder. Besthapu et al. [25] examined the magnetohydrodynamics flow of non-Newtonian nanofluid about a convective stretching surface with thermal radiation and slip effects. Additionally, refer to these related significant studies [26–31].

Casson fluid is an independent of time liquid that is assumed to possess an infinite viscosity when the shear rate is zero. Honey, ketchup, melted chocolate, concentrated fruit juices, and human blood are the most common examples of this liquid. In order to study the behavior of pigment-oil suspensions efficiently, Casson developed a mathematical model in 1959 [32]. This model was one of the most effective and efficient models for predicting the behavior of Casson fluids, which made many researchers employ it to study and analyze these fluids' behavior [21,33–39].

Carbon nanotubes and graphite oxide possess many distinct thermo-physical properties, making them widely used in numerous engineering and physical applications. High thermal conductivity and mechanical strength have earned them superiority over many nanoparticles in improving heat transfer. Two kinds of CNTs, specifically SWCNTs and MWCNTs, are considered in this article; one graphite tube forms the wall of SWCNTs, whereas MWCNTs are more complicated in structure Haq et al. [40] studied the convection slip flow of CNTs about a stretching surface considering magnetic force. Aman et al. [41] studied the free convective flow of carbon nanotubes Maxwell nanofluids. Iqbal et al. [42] investigated the mixed convection CNTs nanofluids flow in a rotating vertical channel under the MHD effect, Hall currents, and radiation.

According to the aforementioned studies for these distinctive nanoparticles, the efforts were directed to examine heat transfer improvement in MHD natural convection flow of methanol as a host Casson nanofluid through graphite oxide and carbon nanotubes past a horizontal curricular cylinder. Furthermore, this study is a development and extension of some previous studies. See [5,43,44]

2. Problem Description

The two-dimensional steady state boundary layer flow of CNTs/GO-Methanol based Casson nanofluid under MHD impact from a horizontal circular cylinder of radius a has been considered. Further, uniform surface heat flux q_w is taken into account. Figure 1 depicts the schematic diagram of the problem, where (ξ^*, η^*) are measured along the circumference of the cylinder at the lower stagnation point $(\xi^* \approx 0)$, and the distance normal to the surface of the cylinder, respectively.

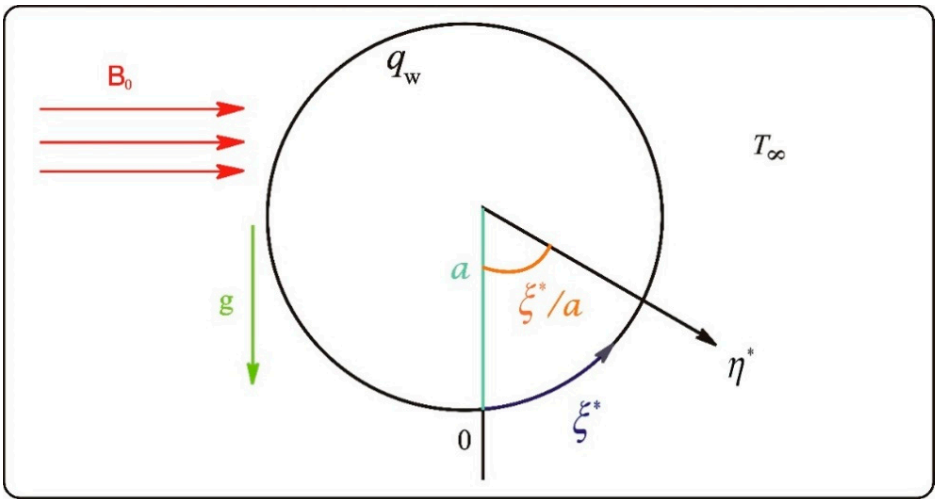

Figure 1. Schematic diagram of the problem.

The system of dimensional partial differential equations that govern our problem is:

$$\frac{\partial u^*}{\partial \xi^*} + \frac{\partial v^*}{\partial \eta^*} = 0, \tag{1}$$

$$u^*\frac{\partial u^*}{\partial \xi^*} + v^*\frac{\partial u^*}{\partial \eta^*} = v_{nf}\left(1+\frac{1}{\gamma}\right)\frac{\partial^2 v^*}{\partial \eta^{*2}} + \left(\frac{\chi\rho_s\beta_s + (1-\chi)\rho_f\beta_f}{\rho_{nf}}\right)g(T-T_\infty)\sin\left(\frac{\xi^*}{a}\right) - \frac{\sigma_{nf}B_0^2}{\rho_{nf}}u^*, \tag{2}$$

$$u^*\frac{\partial T}{\partial \xi^*} + v^*\frac{\partial T}{\partial \eta^*} = \alpha_{nf}\frac{\partial^2 T}{\partial \eta^{*2}}, \tag{3}$$

with dimensional boundary conditions which are given by [43]:

$$\begin{gathered} u^* = v^* = 0,\ \frac{\partial T}{\partial \eta^*} = -\frac{q_w}{k},\ \text{as } \eta^* = 0, \\ u^* \to 0,\ T \to T_\infty,\ \text{ as } \eta^* \to \infty. \end{gathered} \tag{4}$$

The properties of nanofluid are defined by [45]:

$$\begin{gathered} \frac{\sigma_{nf}}{\sigma_f} = 1 + \frac{3(\sigma-1)\chi}{(\sigma+2)-(\sigma-1)\chi},\ \sigma = \frac{\sigma_s}{\sigma_f},\ \frac{k_{nf}}{k_f} = \frac{(k_s+2k_f)-2\chi(k_f-k_s)}{(k_s+2k_f)+\chi(k_f-k_s)},\ \mu_{nf} = \frac{\mu_f}{(1-\chi)^{2.5}}, \\ (\rho c_p)_{nf} = (1-\chi)(\rho c_p)_f + \chi(\rho c_p)_s,\ \rho_{nf} = (1-\chi)\rho_f + \chi\rho_s,\ \alpha_{nf} = \frac{k_{nf}}{(\rho c_p)_{nf}}, \end{gathered} \tag{5}$$

In order to nondimensionalization, the following variables were employed [43]:

$$\begin{gathered} \xi = \frac{\xi^*}{a},\ \eta = Gr^{1/5}\left(\frac{\eta^*}{a}\right),\ u = \left(\frac{a}{\nu_f}\right)Gr^{-2/5}u^*, \\ v = \left(\frac{a}{\nu_f}\right)Gr^{-1/5}v^*,\ \theta = Gr^{1/5}\left(\frac{T-T_\infty}{aq_w/k_f}\right) \end{gathered} \tag{6}$$

where $Gr = g\beta_f(T_w - T_\infty)\frac{a^3}{\nu_f^2}$ is the Grashof number.

By employing Equation (6) into Equations (1)–(4), we obtain the following dimensionless system:

$$\frac{\partial u}{\partial \xi} + \frac{\partial v}{\partial \eta} = 0, \tag{7}$$

$$u\frac{\partial u}{\partial \xi} + v\frac{\partial u}{\partial \eta} = \frac{\rho_f}{(1-\chi)^{2.5}\rho_{nf}}\left(1+\frac{1}{\gamma}\right)\frac{\partial^2 u}{\partial \eta^2} + \left(\frac{\chi\rho_s\beta_s/\beta_f + (1-\chi)\rho_f}{\rho_{nf}}\right)\theta\sin\xi - \frac{\sigma_{nf}\rho_f}{\sigma_f\rho_{nf}}Mu, \tag{8}$$

$$u\frac{\partial \theta}{\partial \xi} + v\frac{\partial \theta}{\partial \eta} = \frac{1}{\Pr}\left(\frac{k_{nf}/k_f}{(1-\chi)+\chi\left(\rho c_p\right)_s/\left(\rho c_p\right)_f}\right)\frac{\partial^2 \theta}{\partial \eta^2}, \tag{9}$$

and the dimensionless boundary conditions are:

$$\begin{array}{c} u = v = 0,\ \frac{\partial \theta}{\partial \eta} = -1 \text{as } \eta = 0, \\ u \to 0,\ \theta \to 0,\ \text{as } \eta \to \infty. \end{array} \tag{10}$$

Here $\Pr = \frac{v_f}{\alpha_f}$ is the Prandtl number, and $M = \left(\frac{\sigma_f B_0^2 a^2 Gr^{\frac{-2}{5}}}{\rho_f v_f}\right)$ is the magnetic parameter.

By using the following transformation [43]:

$$\begin{array}{c} u = \frac{\partial \psi}{\partial \eta} \text{ and } v = -\frac{\partial \psi}{\partial \xi}, \\ \psi = \xi F(\xi,\eta),\ \theta = \theta(\xi,\eta), \end{array} \tag{11}$$

Equations (8)–(10) are reduced to:

$$\begin{array}{c} \frac{\rho_f}{(1-\chi)^{2.5}\rho_{nf}}\left(1+\frac{1}{\gamma}\right)\frac{\partial^3 F}{\partial \eta^3} + F\frac{\partial^2 F}{\partial \eta^2} + \left(\frac{\chi\rho_s\beta_s/\beta_f + (1-\chi)\rho_f}{(1-\chi)\rho_f+\chi\rho_s,}\right)\theta\frac{\sin\xi}{\xi} \\ -\left(\frac{\partial F}{\partial \eta}\right)^2 - \frac{\sigma_{nf}\rho_f}{\sigma_f\rho_{nf}}M\frac{\partial F}{\partial \eta} = \xi\left(\frac{\partial F}{\partial \eta}\frac{\partial^2 F}{\partial \xi\partial \eta} - \frac{\partial F}{\partial \xi}\frac{\partial^2 F}{\partial \eta^2}\right) \end{array} \tag{12}$$

$$\frac{1}{\Pr}\left(\frac{k_{nf}/k_f}{(1-\chi)+\chi\left(\rho c_p\right)_s/\left(\rho c_p\right)_f}\right)\frac{\partial^2 \theta}{\partial \eta^2} + F\frac{\partial \theta}{\partial \eta} = \xi\left(\frac{\partial F}{\partial \eta}\frac{\partial \theta}{\partial \xi} - \frac{\partial F}{\partial \xi}\frac{\partial \theta}{\partial \eta}\right), \tag{13}$$

Subject to:

$$\begin{array}{c} \frac{\partial F}{\partial \eta} = 0,\ F = 0,\ \frac{\partial \theta}{\partial \eta} = -1,\ \text{as } \eta = 0, \\ \frac{\partial F}{\partial \eta} \to 0,\ \theta \to 0\ ,\ \text{as } \eta \to \infty \end{array} \tag{14}$$

at the lower stagnation point of the cylinder ($\xi \approx 0$), we obtained the following ODEs:

$$\frac{\rho_f}{\rho_{nf}}\frac{1}{(1-\chi)^{2.5}}\left(1+\frac{1}{\gamma}\right)F''' + FF'' + \left(\frac{\chi\rho_s\beta_s/\beta_f + (1-\chi)\rho_f}{(1-\chi)\rho_s+\chi\rho_f,}\right)\theta - (F')^2 - \frac{\rho_f}{\rho_{nf}}\frac{\sigma_{nf}}{\sigma_f}M\,F' = 0, \tag{15}$$

$$\frac{1}{\Pr}\left(\frac{k_{nf}/k_f}{(1-\chi)+\chi\left(\rho c_p\right)_s/\left(\rho c_p\right)_f}\right)\theta'' + F\theta' = 0, \tag{16}$$

and the boundary conditions become:

$$\begin{array}{c} F'(0,\eta) = F(0,\eta) = 0,\ \theta'(0) = -1,\ \text{as } \eta = 0\,, \\ F' \to 0,\ \theta \to 0\ ,\ \text{as } \eta \to \infty. \end{array} \tag{17}$$

Two physical quantities are highlighted in the current work, specifically the local skin friction coefficient C_f and local Nusselt number Nu (given by [43,46]):

$$C_f = \left(\frac{\tau_w}{\rho U_\infty^2}\right), \, Nu = \left(\frac{a q_w}{k_f(T_w - T_\infty)}\right), \tag{18}$$

where

$$\tau_w = \mu_{nf}\left(1+\frac{1}{\gamma}\right)\left(\frac{\partial u^*}{\partial \eta^*}\right)_{\eta^*=0}, \, q_w = -k_{nf}\left(\frac{\partial T}{\partial \eta^*}\right)_{\eta^*=0}. \tag{19}$$

By using Equation (7) and the boundary condition in Equation (15), C_f and Nu can be expressed as follows:

$$Gr^{1/5}C_f = \frac{1}{(1-\chi)^{2.5}}\left(1+\frac{1}{\gamma}\right)\xi\frac{\partial^2 F}{\partial \eta^2}(\xi,0), \, Gr^{-1/5}Nu = \frac{k_{nf}}{k_f}\left(\frac{1}{\theta(\xi,0)}\right) \tag{20}$$

3. Numerical Solution

The Keller box method was first addressed by Keller [47]. This method gained an eminence when Jones [48] employed it to solve boundary layer problems. Cebeci and Bradshaw [49] explained the Keller box technique in detail. This method was used in this work to construct a numerical solution.

3.1. The Finite-Difference Method

To reduce the system (12) and (13) into first-order system of equations, we will introduce the following independent variables: $w(\xi,\eta)$, $z(\xi,\eta)$, $t(\xi,\eta)$, and $s(\xi,\eta)$, where $s(\xi,\eta)$, instead of $\theta(\xi,\eta)$, is the variable for temperature, and

$$\begin{aligned} F' &= w, \\ w' &= z, \\ s' &= t, \end{aligned} \tag{21}$$

consequently, Equations (13)–(15) become:

$$\begin{aligned} &\frac{\rho_f}{\rho_{nf}}\frac{1}{(1-\chi)^{2.5}}\left(1+\frac{1}{\gamma}\right)z' + Fz - w^2 - \frac{\rho_f}{\rho_{nf}}\frac{\sigma_{nf}}{\sigma_f}Mw \\ &+\left(\frac{\chi\rho_s\beta_s/\beta_f + (1-\chi)\rho_f}{\rho_{nf}}\right)s\frac{\sin\xi}{\xi} = \xi\left(w\frac{\partial w}{\partial \xi} - z\frac{\partial F}{\partial \xi}\right), \end{aligned} \tag{22}$$

$$\frac{1}{\Pr}\frac{k_{nf}/k_f}{\left((1-\chi)(\rho C_p)_f + \chi\left(\rho c_p\right)_s/\left(\rho c_p\right)_f\right)}t' + Ft = \xi\left(w\frac{\partial s}{\partial \xi} - t\frac{\partial F}{\partial \xi}\right), \tag{23}$$

and the boundary conditions (15) are:

$$\begin{aligned} w(\xi,0) = F(\xi,0) = 0, \text{ and } t(\xi,0) = -1, \\ w(\xi,\infty) = s(\xi,\infty) = 0, \end{aligned} \tag{24}$$

here the primes denoted to differentiation with respect η.

Next, obtain the finite-difference form of Equation (22) about the midpoint $(\xi^n, \eta_{j-1/2})$ of the segment

$$F_j^n - F_{j-1}^n - \frac{h_j}{2}\left(w_j^n + w_{j-1}^n\right) = 0, \tag{25}$$

$$w_j^n - w_{j-1}^n - \frac{h_j}{2}\left(z_j^n + z_{j-1}^n\right) = 0, \tag{26}$$

$$s_j^n - s_{j-1}^n - \frac{h_j}{2}\left(t_j^n + t_{j-1}^n\right) = 0. \tag{27}$$

Finally, center Equations (23) and (24) about the midpoint $(\xi^{n-1/2}, \eta_{j-1/2})$ of the rectangle as follows:

$$\begin{aligned}&\frac{\rho_f}{\rho_{nf}}\frac{1}{(1-\chi)^{2.5}}\left(1+\frac{1}{\gamma}\right)\left(z_j^n - z_{j-1}^n\right) + \left(\frac{1+\alpha}{4}\right)h_j(F_j^n + F_{j-1}^n)(z_j^n + z_{j-1}^n) - \left(\frac{1+\alpha}{4}\right)h_j\,(w_j^n + w_{j-1}^n)^2\\ &-\frac{1}{2}\frac{\rho_f\sigma_{nf}}{\rho_{nf}\sigma_f}Mh_j\,(w_j^n + w_{j-1}^n) + \left(\frac{1+\alpha}{2}\right)h_j z_{j-1/2}^{n-1}(F_j^n + F_{j-1}^n) - \left(\frac{1+\alpha}{2}\right)h_j F_{j-1/2}^{n-1}(z_j^n + z_{j-1}^n)F_{j-1/2}^{n-1}\\ &+\frac{1}{2}\left(\frac{\chi\rho_s\left(\beta_s/\beta_f\right)+(1-\chi)\rho_f}{\rho_{nf}}\right)\frac{\sin\xi^{n-1l2}}{\xi^{n-1l2}}h_j(s_j^n + s_{j-1}^n) = (R_1)_{j-1/2}^{n-1}\end{aligned} \tag{28}$$

$$\begin{aligned}&\frac{1}{\Pr}\frac{k_{nf}/k_f}{\left((1-\chi)(\rho C_p)_f + \chi\left(\rho c_p\right)_s/\left(\rho c_p\right)_f\right)}\left(t_j^n - t_{j-1}^n\right) - \frac{\alpha}{4}h_j(w_j^n + w_{j-1}^n)(s_j^n + s_{j-1}^n)\\ &+\frac{\alpha}{4}h_j(F_j^n + F_{j-1}^n)(t_j^n + t_{j-1}^n) + \frac{\alpha}{2}h_j(w_j^n + w_{j-1}^n)s_{j-1/2}^{n-1} - \frac{\alpha}{2}h_j w_{j-1/2}^{n-1}(s_j^n + s_{j-1}^n)\\ &-\frac{\alpha}{2}h_j(t_j^n - t_{j-1}^n)F_{j-1/2}^{n-1} + \frac{\alpha}{2}h_j t_{j-1/2}^{n-1}(F_j^n + F_{j-1}^n) = (R_2)_{j-1/2}^{n-1}\end{aligned} \tag{29}$$

where

$$(R_1)_{j-1/2}^{n-1} = -h_j\begin{pmatrix}\frac{\rho_f}{\rho_{nf}}\frac{1}{(1-\chi)^{2.5}}\left(1+\frac{1}{\gamma}\right)\frac{\left(z_j^n - z_{j-1}^n\right)}{h_j} + (1-\alpha)F_{j-1/2}^n z_{j-1/2}^n + (\alpha-1)\left(w_{j-1/2}^n\right)^2\\ -\frac{\rho_f\sigma_{nf}}{\rho_{nf}\sigma_f}Mw_{j-1/2}^n + \frac{\chi\rho_s\left(\beta_s/\beta_f\right)+(1-\chi)\rho_f}{\rho_{nf}}\frac{\sin\xi^{n-1l2}}{\xi^{n-1l2}}s_{j-1/2}^n\end{pmatrix}^{n-1}$$

$$(R_2)_{j-1/2}^{n-1} = -h_j\begin{pmatrix}\frac{1}{\Pr}\frac{k_{nf}/k_f}{\left((1-\chi)(\rho C_p)_f + \chi\left(\rho c_p\right)_s/\left(\rho c_p\right)_f\right)}\frac{\left(t_j^n - t_{j-1}^n\right)}{h_j}\\ +(1-\alpha)F_{j-1/2}^n t_{j-1/2}^n + \alpha w_{j-1/2}^n s_{j-1/2}^n\end{pmatrix}^{n-1},\ \alpha = \frac{\xi^{n-1l2}}{k_n}$$

At $\xi = \xi^n$ the boundary conditions become:

$$\begin{aligned}F_0^n = w_0^n = 0,\ \text{and}\ t_0^n = -1\\ w_J^n = s_J^n = 0,\end{aligned} \tag{30}$$

3.2. Newton's Method

The following linearized tridiagonal system was obtained by applying Newton's method to the previous system that consists of Equations (25)–(29):

$$\delta F_j - \delta F_{j-1} - \frac{1}{2}h_j\left(\delta w_j + \delta w_{j-1}\right) = (r_1)_{j-1/2} \tag{31}$$

$$\delta w_j - \delta w_{j-1} - \frac{1}{2}h_j\left(\delta z_j + \delta z_{j-1}\right) = (r_2)_{j-1/2} \tag{32}$$

$$\delta s_j - \delta s_{j-1} - \frac{1}{2}h_j\left(\delta t_j + \delta t_{j-1}\right) = (r_3)_{j-1/2} \tag{33}$$

$$\begin{aligned}&(x_1)_j\delta z_j + (x_2)_j\delta z_{j-1} + (x_3)_j\delta F_j + (x_4)_j\delta F_{j-1} + (x_5)_j\delta w_j\\ &+(x_6)_j\delta w_{j-1} + (x_7)_j\delta s_j + (x_8)_j\delta s_{j-1} = (r_4)_{j-1/2}\end{aligned} \tag{34}$$

$$\begin{aligned}&\left(y_1\right)_j\delta t_j + \left(y_2\right)_j\delta t_{j-1} + \left(y_3\right)_j\delta F_j + \left(y_4\right)_j\delta F_{j-1} + \left(y_5\right)_j\delta w_j\\ &+\left(y_6\right)_j\delta w_{j-1} + \left(y_7\right)_j\delta s_j + \left(y_8\right)_j\delta s_{j-1} = \left(r_5\right)_{j-1/2}\end{aligned} \tag{35}$$

where

$$
\begin{aligned}
(x_1)_j &= \left[\frac{\rho_f}{\rho_{nf}}\frac{1}{(1-\chi)^{2.5}}\left(1+\frac{1}{\gamma}\right)+h_j\left(\frac{(1+\alpha)}{2}F_{j-1/2}-\frac{\alpha}{2}F^{n-1}_{j-1/2}\right)\right]\\
(x_2)_j &= \left[(s_1)_j - 2\frac{\rho_f}{\rho_{nf}}\frac{1}{(1-\chi)^{2.5}}\left(1+\frac{1}{\gamma}\right)\right]\\
(x_3)_j &= h_j\left[\frac{(1+\alpha)}{2}z_{j-1/2}+\frac{\alpha}{2}z^{n-1}_{j-1/2}\right]\\
(x_4)_j &= (x_3)_j\\
(x_5)_j &= h_j\left[-(1+\alpha)w_{j-1/2}-\frac{1}{2}\frac{\rho_f\sigma_{nf}}{\rho_{nf}\sigma_f}M\right]\\
(x_6)_j &= (x_5)_j\\
(x_7)_j &= h_j\left[\frac{1}{2}\left(\frac{\chi\rho_s\left(\beta_s/\beta_f\right)+(1-\chi)\rho_f}{\rho_{nf}}\right)\frac{\sin\xi^{n-1l2}}{\xi^{n-1l2}}\right]\\
(x_8)_j &= (x_7)_j
\end{aligned}
\tag{36}
$$

$$
\begin{aligned}
\left(y_1\right)_j &= \left[\frac{1}{\Pr}\frac{k_{nf}/k_f}{\left((1-\chi)(\rho C_p)_f+\chi\left(\rho c_p\right)_s/\left(\rho c_p\right)_f\right)}+h_j\left(\frac{(1+\alpha)}{2}F_{j-1/2}-\frac{\alpha}{2}F^{n-1}_{j-1/2}\right)\right]\\
\left(y_2\right)_j &= \left[\frac{2}{\Pr}-\left(t_1\right)_j\right]\\
\left(y_3\right)_j &= h_j\left[\frac{(1+\alpha)}{2}t_{j-1/2}+\frac{\alpha}{2}t^{n-1}_{j-1/2}\right]\\
\left(y_4\right)_j &= \left(y_3\right)_j\\
\left(y_5\right)_j &= h_j\left[-\frac{\alpha}{2}s_{j-1/2}+\frac{\alpha}{2}s^{n-1}_{j-1/2}\right]\\
\left(y_6\right)_j &= \left(y_5\right)_j\\
\left(y_7\right)_j &= h_j\left[-\frac{\alpha}{2}w_{j-1/2}-\frac{\alpha}{2}h_j w^{n-1}_{j-1/2}\right]\\
\left(y_8\right)_j &= \left(y_7\right)_j
\end{aligned}
\tag{37}
$$

$$
\begin{aligned}
(r_1)_{j-1/2} &= F_{j-1}-F_j+h_j w_{j-1/2}\\
(r_2)_{j-1/2} &= w_{j-1}-w_j+h_j z_{j-1/2}\\
(r_3)_{j-1/2} &= s_{j-1}-s_j+h_j t_{j-1/2}r\\
(r_4)_{j-1/2} &= -(1+\alpha)h_j F_{j-1/2}z_{j-1/2}+h_j\left(\alpha z_{j-1/2}F^{n-1}_{j-1/2}-\alpha z^{n-1}_{j-1/2}F_{j-1/2}\right)\\
&\quad +h_j\left((1+\alpha)w^2_{j-1/2}+\frac{\rho_f\sigma_{nf}}{\rho_{nf}\sigma_f}Mw_{j-1/2}-\left(\frac{\chi\rho_s\left(\beta_s/\beta_f\right)+(1-\chi)\rho_f}{\rho_{nf}}\right)\frac{\sin\xi^{n-1l2}}{\xi^{n-1l2}}s_{j-1/2}\right)\\
&\quad +\frac{\rho_f}{\rho_{nf}}\frac{1}{(1-\chi)^{2.5}}\left(1+\frac{1}{\gamma}\right)\left(z_{j-1}-z_j\right)+(R_1)^{n-1}_{j-1/2}\\
&\quad r\\
(r_5)_{j-1/2} &= \frac{1}{\Pr}\frac{k_{nf}/k_f}{\left((1-\chi)(\rho C_p)_f+\chi\left(\rho c_p\right)_s/\left(\rho c_p\right)_f\right)}\left(t_{j-1}-t_j\right)-(1+\alpha)h_j F_{j-1/2}t_{j-1/2}\\
&\quad -\alpha h_j t^{n-1}_{j-1/2}F_{j-1/2}+\alpha h_j t_{j-1/2}F^{n-1}_{j-1/2}+\alpha h_j w_{j-1/2}s_{j-1/2}\\
&\quad -\alpha h_j w_{j-1/2}s^{n-1}_{j-1/2}+\alpha h_j w^{n-1}_{j-1/2}s_{j-1/2}+(R_2)^{n-1}_{j-1/2}
\end{aligned}
\tag{38}
$$

3.3. *The Block Tridiagonal Matrix*

The matrix form of the previous linearized tridiagonal system is:

$$\mathbf{X}\boldsymbol{\delta}=\mathbf{r}, \tag{39}$$

where

$$\mathbf{S} = \begin{bmatrix} [X_1] & [C_1] & & & & & \\ [Y_2] & [X_2] & [C_2] & & & & \\ & & & \ddots & & & \\ & & & \ddots & & & \\ & & & \ddots & & & \\ & & & & [Y_{J-1}] & [X_{J-1}] & [C_{J-1}] \\ & & & & & [X_J] & [Y_J] \end{bmatrix}, \ \boldsymbol{\delta} = \begin{bmatrix} [\delta_1] \\ [\delta_2] \\ \vdots \\ [\delta_{J-1}] \\ [\delta_J] \end{bmatrix}, \mathbf{r} = \begin{bmatrix} [r_1] \\ [r_2] \\ \vdots \\ [r_{J-1}] \\ [r_J] \end{bmatrix}.$$

The boundary conditions in Equation (30) are satisfied exactly without iteration, because of these suitable values being kept in every iterate, we suppose that $\delta F_0 = 0,\ \delta w_0 = 0,\ \delta t_0 = 0, \delta w_J = 0, \delta s_J = 0$, by letting $d_J = -\frac{1}{2}h_J$. The elements of matrices are:

$$[X_1] = \begin{bmatrix} 0 & 0 & 1 & 0 & 0 \\ d_1 & 0 & 0 & d_1 & 0 \\ 0 & -1 & 0 & 0 & d_1 \\ (x_2)_1 & (x_8)_1 & (x_3)_1 & (x_1)_1 & 0 \\ 0 & (y_8)_1 & (y_3)_1 & 0 & (y_1)_1 \end{bmatrix} \tag{40}$$

$$\left[X_j\right] = \begin{bmatrix} d_j & 0 & 0 & 0 & 0 \\ -1 & 0 & 0 & 0 & 0 \\ 0 & -1 & 0 & 0 & 0 \\ (x_6)_j & (x_8)_j & (x_3)_j & (x_1)_j & 0 \\ (y_6)_j & (y_8)_j & (y_3)_j & 0 & (y_1)_j \end{bmatrix}, \ 2 \le j \le J, \tag{41}$$

$$\left[Y_j\right] = \begin{bmatrix} 0 & 0 & -1 & 0 & 0 \\ 0 & 0 & 0 & d_j & 0 \\ 0 & 0 & 0 & 0 & d_j \\ 0 & 0 & (x_4)_j & (x_2)_j & 0 \\ 0 & 0 & (y_4)_j & 0 & (y_2)_j \end{bmatrix}, \ 2 \le j \le J, \tag{42}$$

$$\left[C_j\right] = \begin{bmatrix} d_j & 0 & 0 & 0 & 0 \\ 1 & 0 & 0 & 0 & 0 \\ 0 & 1 & 0 & 0 & 0 \\ (x_5)_j & (x_7)_j & 0 & 0 & 0 \\ (y_5)_j & (y_7)_j & 0 & 0 & 0 \end{bmatrix}, \ 1 \le j \le J-1, \tag{43}$$

$$[\delta_1] = \begin{bmatrix} \delta z_0 \\ \delta s_0 \\ \delta F_1 \\ \delta z_1 \\ \delta t_1 \end{bmatrix}, \left[\delta_j\right] = \begin{bmatrix} \delta w_{j-1} \\ \delta s_{j-1} \\ \delta F_{j-1} \\ \delta z_{j-1} \\ \delta t_{j-1} \end{bmatrix}, 2 \le j \le J, \ \left[r_j\right] = \begin{bmatrix} (r_1)_{j-(1/2)} \\ (r_2)_{j-(1/2)} \\ (r_3)_{j-(1/2)} \\ (r_4)_{j-(1/2)} \\ (r_5)_{j-(1/2)} \end{bmatrix}, 1 \le j \le J \tag{44}$$

The system in Equation (41) is solved by the Lower-Upper (LU) factorization method. Numerical calculations are carried out via MATLAB software version 7. The convergence criterion is assumed to be the wall shear stress $z(\xi, 0)$ as recommended by Cebeci and Bradshaw [49], hence, the calculations processes iterate until satisfying the convergence criterion, and stopped when $\left|\delta z_0^{(i)}\right| < \varepsilon_1$, where ε_1 is chosen to be 10^{-7} which provides accurate values up to six decimal places.

4. Results and Discussion

With a view to achieving a fine insight for significant features of the flow and the heat transfer characteristics, numerical computations for various values of nanoparticles volume fraction, Casson and magnetic parameters were carried out, and its representation was performed graphically via MATLAB software.

4.1. Validation of Results

To validate our numerical procedure and to confirm that our approach is suitable for the examination issue, comparisons for local skin friction coefficient $Gr^{1/5}C_f$ and surface temperature $\theta_w(\xi, 0)$ with numerical findings in the prior literature has been made, the obtained outcomes achieved a close agreement with previously published results by Merkin and Pop [5], Molla et al. [43] and Alkasasbeh et al. [44] as shown in Tables 1 and 2.

Table 1. Comparison of the current findings $Gr^{1/5}C_f$ with prior published findings, at $\Pr = 1,\ \chi = 0,\ M = 0,$ and $\gamma \to \infty$.

ξ	Merkin and Pop [5]	Molla et al. [43]	Alkasasbeh et al. [44]	Present
0	0.000	0.000	0.0000	0.0000
0.2	0.274	0.272	0.2732	0.2727
0.6	0.795	0.789	0.7947	0.7924
1	1.241	1.226	1.2351	1.237
1.6	1.671	1.637	1.6679	1.6642
2	1.744	1.693	1.7394	1.7349
2.6	1.451	1.370	1.4447	1.4391
3	0.913	0.797	0.9046	0.8977
π	0.613	0.585	0.6068	0.5733

Table 2. Comparison of the current findings for surface temperature $\theta_w(\xi, 0)$ with prior published findings, at $\Pr = 1,\ \chi = 0,\ M = 0,$ and $\gamma \to \infty$.

ξ	Merkin and Pop [5]	Molla et al. [43]	Alkasasbeh et al. [44]	Present
0	1.996	1.996	1.9964	1.9966
0.2	1.999	1.999	1.9985	1.9984
0.6	2.014	2.015	2.0127	2.0127
1	2.043	2.047	2.0436	2.0422
1.6	2.120	2.129	2.1225	2.1207
2	2.202	2.216	2.2064	2.2035
2.6	2.403	2.430	2.4128	2.4069
3	2.660	2.716	2.6807	2.6680
π	2.824	2.841	2.8284	2.8519

4.2. Graphical Results and Discussion

The range of the parameters for the computational simulations have been considering as: nanoparticles volume fraction $(0.1 \leq \chi \leq 0.2)$, magnetic parameter $(0.5 \leq M \leq 3)$ and Casson parameter $(\gamma > 0)$. Table 3 displays the thermo-physical properties of methanol and nanoparticles.

Table 3. Thermo-physical properties of nanoparticles and methanol [45,50,51].

Thermo-Physical Property	Methanol	SWCNTs	MWCNTs	GO
$\rho\left(kg/m^3\right)$	792	2600	1600	1800
$C_p(J/kgK)$	2545	425	796	717
$k(w/mK)$	0.2035	6600	3000	5000
$\beta \times 10^{-5}\left(K^{-1}\right)$	149	27	44	28.4
$\sigma(s/m)$	0.5×10^{-6}	10^{-6}	1.9×10^{-4}	1.1×10^{-5}
Pr	7.38	-	-	-

Figures 2 and 3 reveal the impact of nanoparticle volume fraction χ on temperature and velocity, respectively. It is found from these figures that a rise in χ leads to enhance the temperature and velocity; this occurs because an increment χ improves the convection from the cylinder to methanol and the energy transmission, therefore increases the temperature and velocity. This can be demonstrated when the thermal conductivity of nanofluids increases as the solid nanoparticles enlarge which are having a great thermal conductivity than the base fluid. Hence, the heat transfer from the base fluid to solid nanoparticles is greater and magnifies the temperature of the nanofluid. Further, it is depicted that the nanofluid temperature increases sufficiently with increasing values of χ for SWCNTs as well as for GO than in the case of MWCNTs. Substantially, this is due to the cause that a rise in χ indications to a growth in the thermal conductivity of SWCNTs/Go nanofluid, and hereafter the viscosity of the thermal boundary layer elevates.

Figures 4 and 5 illustrate that the nanoparticle volume fraction χ is directly proportional to both local skin friction coefficient $Gr^{1/5}C_f$ and local Nusselt number. Augmentation in the value of χ improves thermal conductivity and density of methanol, thereby enhancing $Gr^{-1/5}Nu$ and $Gr^{1/5}C_f$. This is due to the fact that, with increasing the values of nanoparticle volume fraction parameter, both the momentum and thermal boundary layer thickness grows as mentioned in Figures 4 and 5. This means the skin friction and the heat transfer rate intensifies in the nanofluids area when the volume fraction of nanoparticle χ augments.

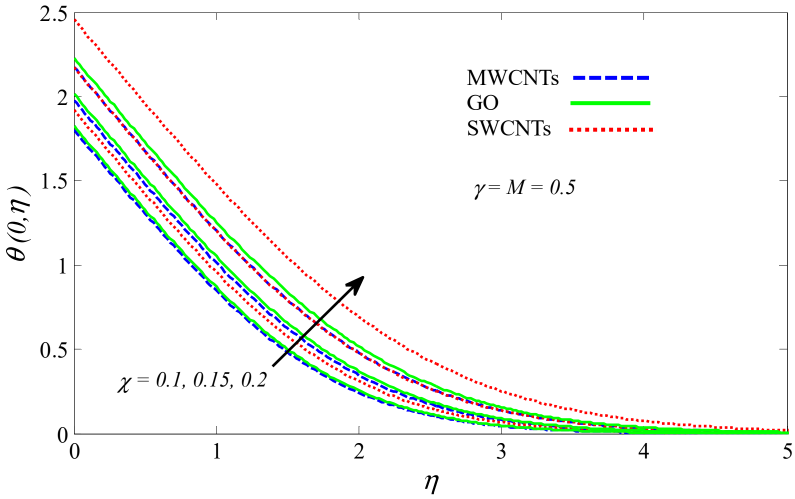

Figure 2. Impact of χ on θ.

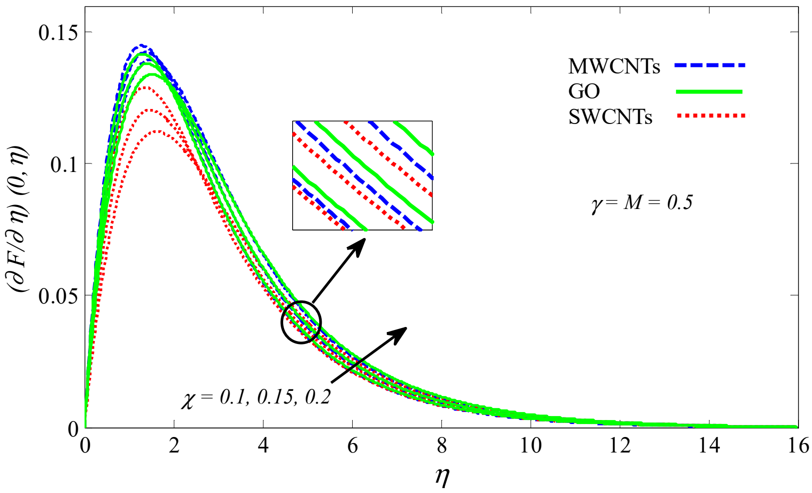

Figure 3. Impact of χ on $\partial F/\partial \eta$.

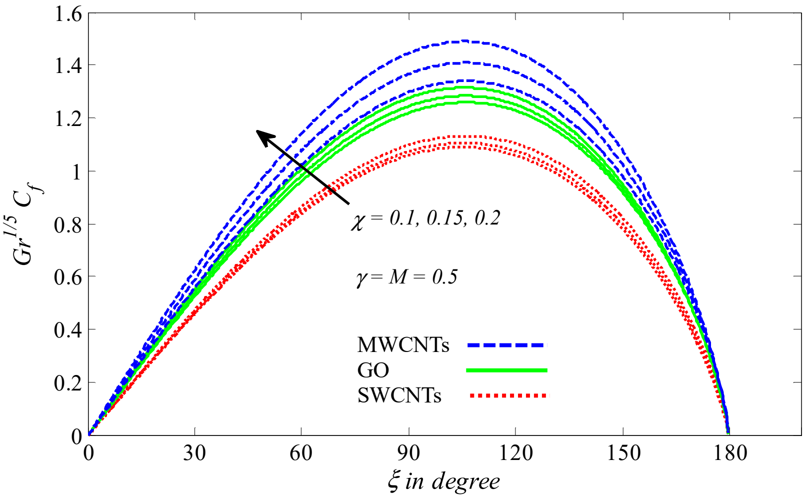

Figure 4. Impact of χ on $Gr^{1/5}C_f$.

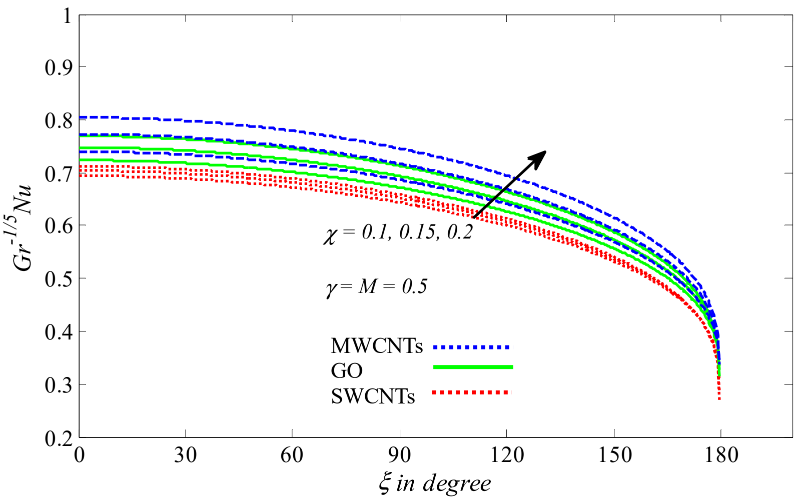

Figure 5. Impact of χ on $Gr^{-1/5}Nu$.

Figures 6 and 7 evidence that with rising the Casson parameter γ, the temperature and velocity decrease. Actually, growing values of γ generate resistance forces that act to inhibit the fluid's velocity. Physically, a greater and smaller value of γ corresponds to Newtonian and non-Newtonian fluids, respectively (i.e., γ decreases the yield stress). However, it agrees with the stated physical analogy, which is due to the temperature injected that influences the nanofluid temperature.

Figures 8 and 9 portray the effect of the Casson parameter γ on both local skin friction coefficient $Gr^{1/5}C_f$ and local Nusselt numb $Gr^{-1/5}Nu$. It can be observed that at higher values of the Casson parameter, the yield stress decreases, causing a decrease in skin friction, while the reverse happens with the Nusselt number. This is because, as mentioned above, greater values of γ are accompanied by lower in the yield stress of the Casson fluid, which causes a reduction in rheological characteristics. Therefore, the flow approaches closer to Newtonian conduct and the fluid is able to shear slower along the cylinder surface. Consequently, the Nusselt number is found to enhance as γ is boosted. This occurs with the above data on temperature distribution as explored in Figure 7.

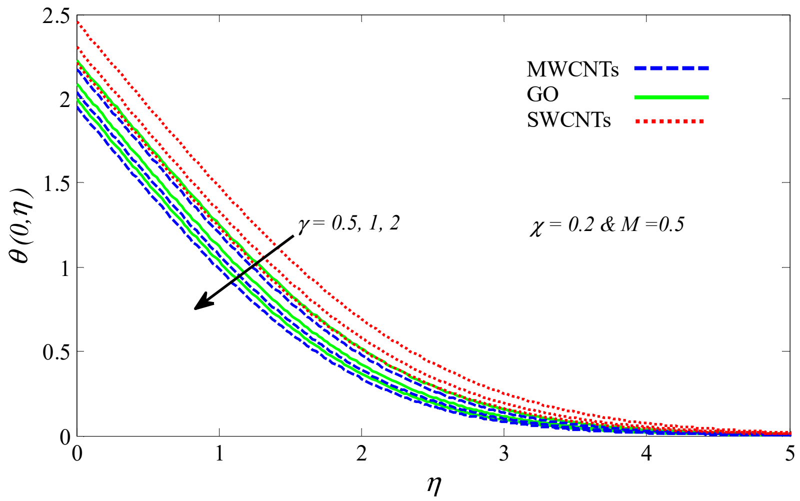

Figure 6. Impact of γ on θ.

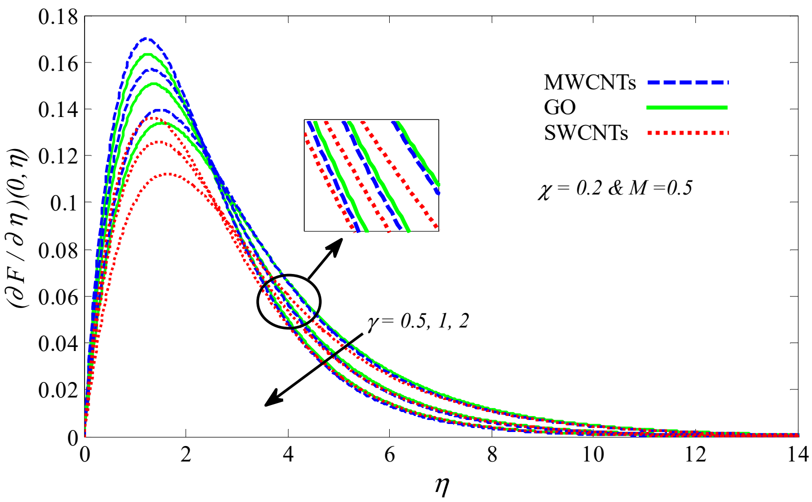

Figure 7. Impact of γ on $\partial F/\partial\eta$.

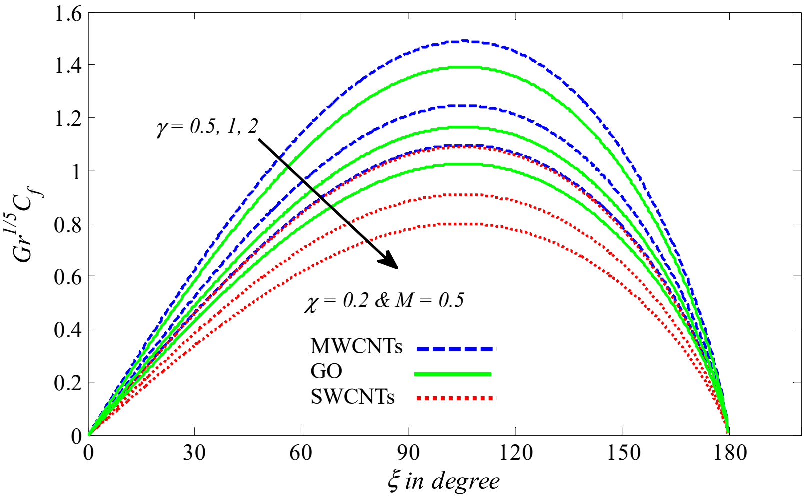

Figure 8. Impact of γ on $Gr^{1/5}C_f$.

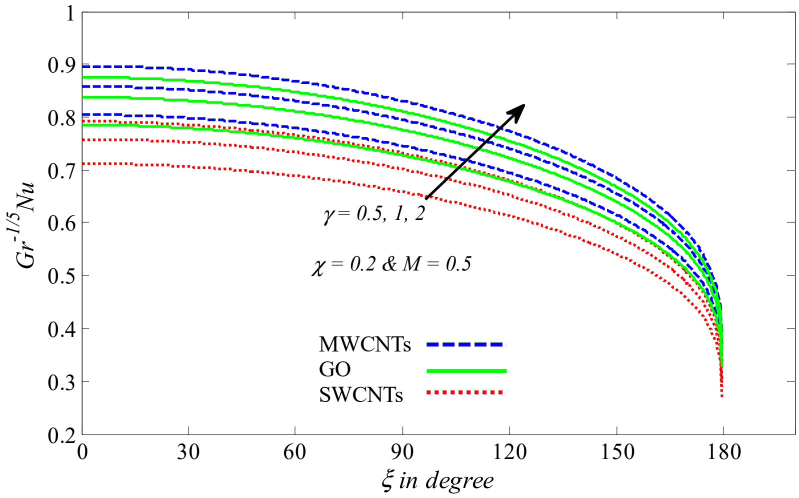

Figure 9. Impact of γ on $Gr^{-1/5}Nu$.

In Figures 10 and 11, the influence of the magnetic field M on both temperature and velocity are elaborated. It is noted here that Lorentz force formed by the growth of the magnetic field decelerates velocity and enhances the temperature. In fact, a magnetic field yields a drag-like force; namely, the Lorentz force. This force acts in the opposite direction, which results in the reduction in velocity, and the fluid temperature boosts by magnifying the strength of the magnetic field.

In Figures 12 and 13, both the skin friction coefficient and local Nusselt number declined with increasing values of the magnetic parameter M. This is attributable to the fact that as the intensity of the magnetic field rises, the motion of the fluid is inhibited as a result of the generation of Lorentz force. This leads to the argument that an applied magnetic field tends to heat the nanoliquid, and thus heat transfer from the cylinder reduces, and then both local skin friction coefficient $Gr^{1/5}C_f$ and local Nusselt number $Gr^{-1/5}Nu$ reduce. All of this happens due to Lorentz force in the visualization of the transverse applied magnetic field opposing the transport phenomena and slowing down the fluid movement. No doubt, the magnetic can be utilized as a beneficial agent for controlling the flow and heat transfer characteristics. Moreover, the graphical findings revealed that MWCNTs - methanol generated the highest heat transfer rate, skin friction, and velocity, as well as it had the lowest temperature, this is due to the unmatched thermal properties that possess MWCNTs.

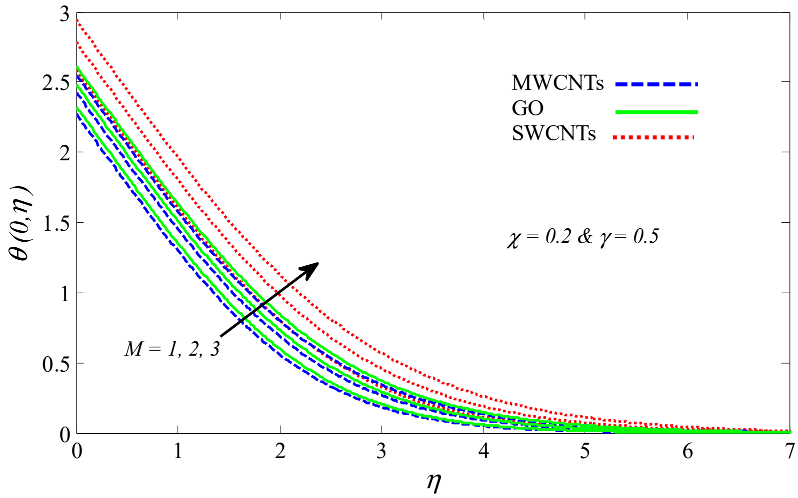

Figure 10. Impact of M on θ.

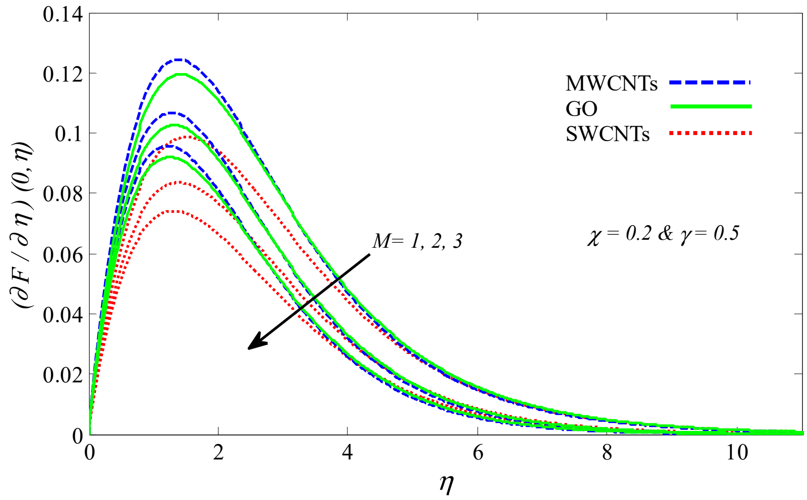

Figure 11. Impact of M on $\partial F/\partial\eta$.

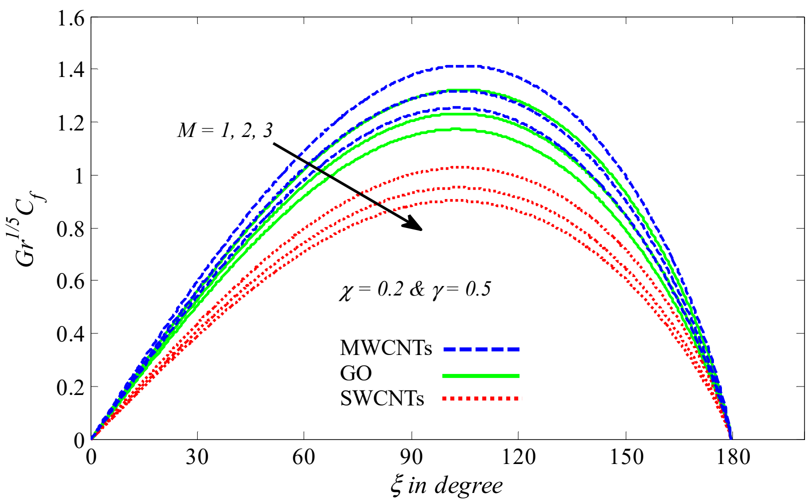

Figure 12. Impact of M on $Gr^{1/5}C_f$.

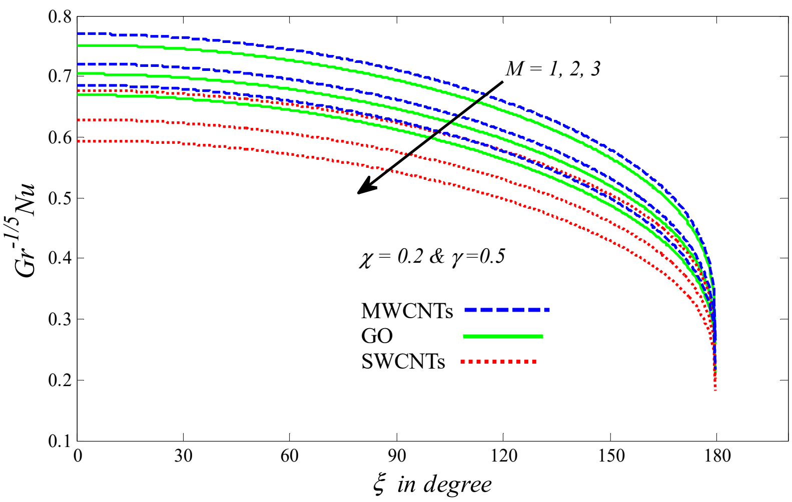

Figure 13. Impact of M on $Gr^{-1/5}Nu$.

5. Conclusions

In the current examination, the magnetohydrodynamics natural convection flow of Graphite oxide/Carbon nanotubes—Methanol based Casson nanofluids past a horizontal curricular cylinder is presented. Tiwari-Das's model is employed to consider the volume fraction of nanoparticles in the computational simulations. On the other hand, uniform heat flux is taken into account. However, the outcomes exposed that the multiple walls carbon nanotubes produce the most effective heat transfer performance, it also gave the highest velocity and lowest temperature to the host Casson liquid. Temperature and velocity profiles confirmed that a rise in χ leads to enhancing temperature and velocity, while with rising the Casson parameter γ, the temperature and velocity decrease. The magnetic field M had a positive effect on the temperature and an inverse effect on the velocity. Augmentation in the value of χ improved $Gr^{-1/5}Nu$ and $Gr^{1/5}C_f$, both the $Gr^{-1/5}Nu$ and $Gr^{1/5}C_f$ declined with increasing values of the magnetic parameter. We also found that $Gr^{1/5}C_f$ is a decreasing function of Casson parameter γ while $Gr^{-1/5}Nu$ is an increasing function of it.

Author Contributions: A.S.H. and F.A.A.: Formal analysis, Investigation, and Methodology; F.A.A. and H.T.A.: Software; A.S.H., H.T.A., A.M.R. and R.I.: Validation; A.S.H., H.T.A., A.M.R. and R.I.: Writing—review and editing. All authors have read and agreed to the published version of the manuscript.

Funding: This project was supported by the Deanship of Scientific Research at Prince Sattam Bin Abdulaziz University under the research project # 2020/01/16361.

Conflicts of Interest: The authors declare no conflict of interest.

Nomenclature

a	Radius of Cylinder	α	Thermal diffusivity
B_0	Magnetic field strength	γ	Casson parameter
C_f	Skin friction coefficient	β_f	Thermal expansion of base fluid
Gr	Grashof number	β_s	Thermal expansion of nanoparticles
g	Gravity vector	θ	Temperature of nanofluid
k	Thermal conductivity	μ_β	Plastic Dynamic viscosity of base fluid
M	Magnetic parameter	μ_f	Dynamic viscosity of base fluid
Nu	Nusselt Number	ρ	Density
Pr	Prandtl number	$\left(\rho c_p\right)$	Heat capacity
p_y	Yield stress	τ_w	Wall shear stress
q_w	Wall heat flux	χ	Nanoparticle volume fraction

T	Temperature of the fluid	ψ	Stream function
T_∞	Ambient temperature	σ	Electrical conductivity
u	ξ—component of velocity	Subscript	
v	η—component of velocity	s	nanoparticles
v_f	Kinematic viscosity	nf	Nanofluid
Greek symbols		f	Base fluid

References

1. Blasius, H. Grenzschichten in Flumigkeiten Mit Kleiner Reibung. *Z. Math. Phys.* **1908**, *56*, 1–37.
2. Frossling, N. Calculation by series expansion of the heat transfer in laminar, constant-property boundary layers at nonisothermal surfaces. *Ark. Fys.* **1958**, *14*. Available online: https://www.osti.gov/biblio/4314587 (accessed on 10 October 2020).
3. Merkin, J. Free convection boundary layer on an isothermal horizontal cylinder. In Proceedings of the American Society of Mechanical Engineers and American Institute of Chemical Engineers, Heat Transfer Conference, St. Louis, MO, USA, 9–11 August 1976.
4. Merkin, J. Mixed convection from a horizontal circular cylinder. *Int. J. Heat Mass Transf.* **1977**, *20*, 73–77. [CrossRef]
5. Merkin, J.; Pop, I. A note on the free convection boundary layer on a horizontal circular cylinder with constant heat flux. *Heat Mass Transf.* **1988**, *22*, 79–81. [CrossRef]
6. Nazar, R.; Amin, N.; Pop, I. Mixed convection boundary-layer flow from a horizontal circular cylinder in micropolar fluids: Case of constant wall temperature. *Int. J. Numer. Method H* **2003**, *13*, 86–109. [CrossRef]
7. Anwar, I.; Amin, N.; Pop, I. Mixed convection boundary layer flow of a viscoelastic fluid over a horizontal circular cylinder. *Int. J. Nonlin. Mech.* **2008**, *43*, 814–821. [CrossRef]
8. Mabood, F.; Khan, W.; Yovanovich, M. Forced convection of nanofluid flow across horizontal circular cylinder with convective boundary condition. *J. Mol. Liq.* **2016**, *222*, 172–180. [CrossRef]
9. Rao, A.S.; Amanulla, C.; Nagendra, N.; Beg, O.A.; Kadir, A. Hydromagnetic flow and heat transfer in a Williamson Non-Newtonian fluid from a Horizontal circular cylinder with Newtonian Heating. *Int. J. Appl. Comput. Math.* **2017**, *3*, 3389–3409.
10. Ingham, D.; Pop, I. Natural convection about a heated horizontal cylinder in a porous medium. *J. Fluid Mech.* **1987**, *184*, 157–181. [CrossRef]
11. Nazar, R.; Amin, N.; Pop, I. Mixed convection boundary-layer flow from a horizontal circular cylinder with a constant surface heat flux. *Heat Mass Transf.* **2004**, *40*, 219–227. [CrossRef]
12. Ibrahim, F.; Hamad, M. Group method analysis of mixed convection boundary-layer flow of a micropolar fluid near a stagnation point on a horizontal cylinder. *Acta Mech.* **2006**, *181*, 65–81. [CrossRef]
13. Gorla, R.S.R.; El-Kabeir, S.; Rashad, A. Heat transfer in the boundary layer on a stretching circular cylinder in a nanofluid. *J. Heat Transf.* **2011**, *25*, 183–186. [CrossRef]
14. Chamkha, A.J.; Rashad, A.; Aly, A.M. Transient natural convection flow of a nanofluid over a vertical cylinder. *Meccanica* **2013**, *48*, 71–81. [CrossRef]
15. Rashad, A.; Chamkha, A.; Modather, M. Mixed convection boundary-layer flow past a horizontal circular cylinder embedded in a porous medium filled with a nanofluid under convective boundary condition. *Comput. Fluids* **2013**, *86*, 380–388. [CrossRef]
16. Tlili, I.; Khan, W.; Ramadan, K. MHD Flow of Nanofluid Flow Across Horizontal Circular Cylinder: Steady Forced Convection. *J. Nanofluids* **2019**, *8*, 179–186. [CrossRef]
17. Rashad, A.; Nabwey, H.A. Gyrotactic mixed bioconvection flow of a nanofluid past a circular cylinder with convective boundary condition. *J. Taiwan Inst. Chem. Eng.* **2019**, *99*, 9–17. [CrossRef]
18. Chamkha, A.J.; Aly, A. MHD free convection flow of a nanofluid past a vertical plate in the presence of heat generation or absorption effects. *Chem. Eng. Commun.* **2010**, *198*, 425–441. [CrossRef]
19. Hamad, M.; Pop, I.; Ismail, A.M. Magnetic field effects on free convection flow of a nanofluid past a vertical semi-infinite flat plate. *Nonlinear Anal. Real World Appl.* **2011**, *12*, 1338–1346. [CrossRef]
20. Rana, P.; Dhanai, R.; Kumar, L. MHD slip flow and heat transfer of Al2O3-water nanofluid over a horizontal shrinking cylinder using Buongiorno's model: Effect of nanolayer and nanoparticle diameter. *Adv. Powder Technol.* **2017**, *28*, 1727–1738. [CrossRef]

21. Alwawi, F.A.; Alkasasbeh, H.T.; Rashad, A.M.; Idris, R. A numerical approach for the heat transfer flow of carboxymethyl cellulose-water based Casson nanofluid from a solid sphere generated by mixed convection under the influence of Lorentz force. *Mathematics* **2020**, *8*, 1094. [CrossRef]
22. Choi, S.U.; Eastman, J.A. *Enhancing Thermal Conductivity of Fluids with Nanoparticles*; Argonne National Laboratory: DuPage County, IL, USA, 1995.
23. Akbar, N.S.; Nadeem, S.; Haq, R.U.; Khan, Z. Radiation effects on MHD stagnation point flow of nano fluid towards a stretching surface with convective boundary condition. *Chin. J. Aeronaut.* **2013**, *26*, 1389–1397. [CrossRef]
24. Dhanai, R.; Rana, P.; Kumar, L. MHD mixed convection nanofluid flow and heat transfer over an inclined cylinder due to velocity and thermal slip effects: Buongiorno's model. *Powder Technol.* **2016**, *288*, 140–150. [CrossRef]
25. Besthapu, P.; Haq, R.U.; Bandari, S.; Al-Mdallal, Q.M. Thermal radiation and slip effects on MHD stagnation point flow of non-Newtonian nanofluid over a convective stretching surface. *Neural Comput. Appl.* **2019**, *31*, 207–217. [CrossRef]
26. Wang, X.-Q.; Mujumdar, A.S. Heat transfer characteristics of nanofluids: A review. *Int. J. Sci.* **2007**, *46*, 1–19. [CrossRef]
27. Buongiorno, J. Convective transport in nanofluids. *J. Heat Transf.* **2006**, *128*, 240–250. [CrossRef]
28. Tiwari, R.K.; Das, M.K. Heat transfer augmentation in a two-sided lid-driven differentially heated square cavity utilizing nanofluids. *Int. J. Heat Mass Transf.* **2007**, *50*, 2002–2018. [CrossRef]
29. Swalmeh, M.Z.; Alkasasbeh, H.T.; Hussanan, A.; Mamat, M. Heat transfer flow of Cu-water and Al2O3-water micropolar nanofluids about a solid sphere in the presence of natural convection using Keller-box method. *Res. Phys.* **2018**, *9*, 717–724. [CrossRef]
30. Swalmeh, M.Z.; Alkasasbeh, H.T.; Hussanan, A.; Nguyen Thoi, T.; Mamat, M. Microstructure and inertial effects on natural convection micropolar nanofluid flow about a solid sphere. *Int. J. Ambient. Energy* **2019**, 1–12. [CrossRef]
31. Alwawi, F.A.; Alkasasbeh, H.T.; Rashad, A.; Idris, R. Heat transfer analysis of ethylene glycol-based Casson nanofluid around a horizontal circular cylinder with MHD effect. *Proc. Inst. Mech. Eng. Part C* **2020**, *234*, 2569–2580. [CrossRef]
32. Casson, N. A flow equation for pigment-oil suspensions of the printing ink type. *Rheol. Disperse Syst.* **1959**, *2*, 84–102.
33. Mustafa, M.; Hayat, T.; Pop, I.; Aziz, A. Unsteady boundary layer flow of a Casson fluid due to an impulsively started moving flat plate. *Heat. Transf. Asian. Res.* **2011**, *40*, 563–576. [CrossRef]
34. Khalid, A.; Khan, I.; Khan, A.; Shafie, S. Unsteady MHD free convection flow of Casson fluid past over an oscillating vertical plate embedded in a porous medium. *Eng. Sci. Technol. Int. J.* **2015**, *18*, 309–317. [CrossRef]
35. EL-Kabeir, S.; El-Zahar, E.; Rashad, A. Effect of chemical reaction on heat and mass transfer by mixed convection flow of casson fluid about a sphere with partial slip. *J Comput. Nanos.* **2016**, *13*, 5218–5226. [CrossRef]
36. Hussanan, A.; Salleh, M.Z.; Alkasasbeh, H.T.; Khan, I. MHD flow and heat transfer in a Casson fluid over a nonlinearly stretching sheet with Newtonian heating. *Heat Transf. Res.* **2018**, *49*, 1185–1198. [CrossRef]
37. Alwawi, F.A.; Alkasasbeh, H.T.; Rashad, A.M.; Idris, R. Natural convection flow of Sodium Alginate based Casson nanofluid about a solid sphere in the presence of a magnetic field with constant surface heat flux. In Proceedings of the Journal of Physics, Conference Series, Kuantan, Malaysia, 23–25 July 2019; p. 012005.
38. Haldar, S.; Mukhopadhyay, S.; Layek, G. Flow and heat transfer of Casson fluid over an exponentially shrinking permeable sheet in presence of exponentially moving free stream with convective boundary condition. *Mech. Adv. Mater. Struct.* **2019**, *26*, 1498–1504. [CrossRef]
39. Alwawi, F.A.; Alkasasbeh, H.T.; Rashad, A.; Idris, R. MHD natural convection of Sodium Alginate Casson nanofluid over a solid sphere. *Res. Phys.* **2020**, *16*, 102818. [CrossRef]
40. Haq, R.U.; Nadeem, S.; Khan, Z.H.; Noor, N.F.M. Convective heat transfer in MHD slip flow over a stretching surface in the presence of carbon nanotubes. *Phys. B* **2015**, *457*, 40–47. [CrossRef]
41. Aman, S.; Khan, I.; Ismail, Z.; Salleh, M.Z.; Al-Mdallal, Q.M. Heat transfer enhancement in free convection flow of CNTs Maxwell nanofluids with four different types of molecular liquids. *Sci. Rep.* **2017**, *7*, 2445. [CrossRef] [PubMed]

42. Iqbal, Z.; Akbar, N.; Azhar, E.; Maraj, E. MHD rotating transport of CNTS in a vertical channel submerged with Hall current and oscillations. *Eur. Phys. J. Plus* **2017**, *132*, 143. [CrossRef]
43. Molla, M.M.; Paul, S.C.; Hossain, M.A. Natural convection flow from a horizontal circular cylinder with uniform heat flux in presence of heat generation. *Appl. Math. Model.* **2009**, *33*, 3226–3236. [CrossRef]
44. Alkasasbeh, H.T.; Swalmeh, M.Z.; Hussanan, A.; Mamat, M. Numerical Solution of Heat Transfer Flow in Micropolar Nanofluids with Oxide Nanoparticles in Water and Kerosene Oil about a Horizontal Circular Cylinder. *IAENG Int. J. Appl. Math.* **2019**, *49*, 1–8.
45. Zangooee, M.; Hosseinzadeh, K.; Ganji, D. Hydrothermal analysis of MHD nanofluid (TiO2-GO) flow between two radiative stretchable rotating disks using AGM. *Case Stud. Eng.* **2019**, *14*, 100460. [CrossRef]
46. Dero, S.; Mohd Rohni, A.; Saaban, A. Effects of the viscous dissipation and chemical reaction on Casson nanofluid flow over the permeable stretching/shrinking sheet. *Heat Transf.* **2020**, *49*, 1736–1755. [CrossRef]
47. Keller, H.; Bramble, J. *Numerical Solutions of Partial Differential Equations*; Academic Press: New York, NY, USA, 1970.
48. Jones, E. An asymptotic outer solution applied to the Keller box method. *J. Comput. Phys.* **1981**, *40*, 411–429. [CrossRef]
49. Cebeci, T.; Bradshaw, P. *Physical and Computational Aspects of Convective Heat Transfer*; Springer Science & Business Media: New York, NY, USA, 2012; p. 487.
50. Reddy, J.R.; Sugunamma, V.; Sandeep, N. Impact of nonlinear radiation on 3D magnetohydrodynamic flow of methanol and kerosene based ferrofluids with temperature dependent viscosity. *J. Mol. Liq.* **2017**, *236*, 93–100. [CrossRef]
51. Khalid, A.; Khan, I.; Khan, A.; Shafie, S.; Tlili, I. Case study of MHD blood flow in a porous medium with CNTS and thermal analysis. *Case Stud. Eng.* **2018**, *12*, 374–380. [CrossRef]